Analysis of Signal Propagation Through TSVs Within Distilled Water for Liquid-Cooled Microsystems

Hanju Oh, *Student Member, IEEE*, Gary S. May, *Fellow, IEEE*, and Muhannad S. Bakir, *Senior Member, IEEE*

***Abstract*— This paper analyzes the impact of liquid cooling on the electrical characteristics of through-silicon vias (TSVs) using a microfluidic cooling testbed containing TSVs. The microfabrication of TSVs in a silicon micropin-fin heat sink is presented, and the high-frequency characterization of TSVs within a micropin-fin heat sink using distilled water is performed from 10 MHz to 20 GHz. TSV capacitance and conductance are extracted from measurements; TSVs within distilled water have larger capacitance and conductance than TSVs in silicon due to the lossy characteristics of distilled water at high frequencies. A coaxial-like TSV configuration, which consists of multiple ground TSVs surrounding a center signal TSV, is proposed and demonstrated to shield signal TSVs from the coolant.**

***Index Terms*— 3-D integrated circuits (3-D ICs), coaxial TSVs, microfluidic cooling, through-silicon vias (TSVs).**

I. Introduction

TO ATTAIN high-bandwidth and low-power communication between integrated circuits (ICs), 2.5-D and 3-D ICs have recently received significant attention [1]. The advantages of 2.5-D and 3-D ICs include enabling the heterogeneous integration of logic, high-bandwidth memory, RF ICs, and field-programmable gate array (FPGA) applications within a single package. However, such stacked ICs generally suffer from a thermal bottleneck due to the innate difficulty of dissipating the generated heat inside the stack [2]. To address heat removal, microfluidic cooling has been widely explored due to its high cooling capability over conventional air cooling technology [3]. Microfluidic cooling was introduced in [4] and, since then, it has been widely studied with numerous heat sink structures [2]–[5]. Moreover, the integration of microfluidic cooling with 3-D microsystems has been reported using a through-silicon via (TSV) technology [6], [7].

As the need for microfluidic cooling in some applications increases, there have been various studies to understand the frequency-dependent electrical characteristics of coolants used in microfluidic cooling. It is well known that the permittivity of distilled water changes significantly with frequency [8], [9]. The complex permittivity (real and imaginary permittivities) of distilled water has been characterized as a function of frequency using microwave double-beam interferometers [10]. In addition, microwave platforms, such as ring resonators and RF sensing devices, have been developed to measure the permittivity of distilled water [11], [12]. Moreover, this frequency-dependent permittivity behavior of distilled water has been purposely utilized in various microwave components. For example, an L-band filter was integrated with microfluidic cooling to demonstrate a tunable corner frequency of the filter with respect to its dielectric constant [13]. In a similar manner, a high-sensitivity tunable sensor with conductor-backed coplanar waveguide (CPW) configuration was integrated with distilled water and a methanol-water solution [14]. A wideband differential detector was presented for the quantitative extraction of the frequency-dependent dielectric properties of different liquids [15]. One research study presented a shielded CPW on a liquid crystal polymer substrate with embedded distilled water to demonstrate the RF isolation of the CPW from the water [16]. However, no prior study has analyzed the impact of liquid cooling on the signal propagation of TSVs. The impact of the coolant on the electrical signaling should be analyzed, especially for liquid-cooled microsystems, because, in such systems, the liquid coolant surrounds the TSVs within a microfluidic heat sink [17]. The presence of coolant between signal and ground TSVs will impact electrical signal propagation, including loss, signal integrity, and crosstalk [18].

To address this need, this paper analyzes the impact of distilled water on the electrical performance of TSVs by extracting the capacitance and conductance of TSVs within distilled water. This paper is organized as follows. Section II presents the equivalent circuit models of TSVs in a silicon substrate and TSVs in a micropin-fin heat sink filled with distilled water. Section III describes the microfabrication of a testbed containing TSVs in silicon micropin-fins. Section IV analyzes the electrical performance of TSVs within distilled water compared with conventional TSVs in silicon. In Section V, we propose a coaxial-like TSV configuration within a microfluidic heat sink as a possible solution to minimize the impact of coolant properties on the TSVs. Finally, the conclusion is drawn in Section VI.

II. Design of TSVs in a Micropin-Fin Heat Sink Within Distilled Water

Fig. 1 shows two examples of high-performance microsystems with integrated liquid cooling: 1) logic and FPGA dice stacked on a microfluidic-cooled silicon interposer and 2) 3-D integration of logic and FPGA dice with integrated

Manuscript received November 13, 2015; revised January 6, 2016; accepted January 7, 2016. Date of publication February 12, 2016; date of current version February 23, 2016. This work was supported by the Defense Advanced Research Projects Agency under Grant HR0011-13-2-0008. The review of this paper was arranged by Editor M. M. Hussain.

The authors are with the School of Electrical and Computer Engineering, Georgia Institute of Technology, Atlanta, GA 30332 USA (e-mail: hanju.oh@gatech.edu; gary.may@coe.gatech.edu; muhannad.bakir@mirc.gatech.edu).

Color versions of one or more of the figures in this paper are available online at http://ieeexplore.ieee.org.

Digital Object Identifier 10.1109/TED.2016.2519023

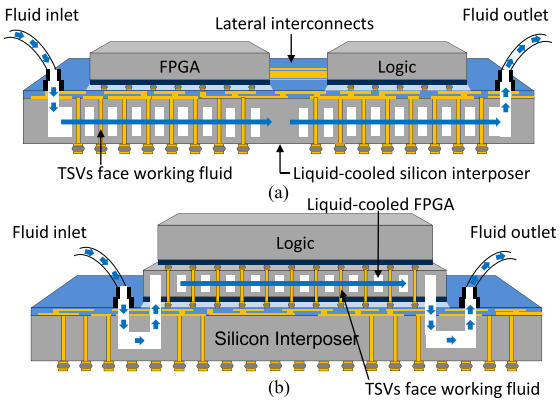

Fig. 1. Envisioned silicon microsystems with integrated microfluidic cooling for FPGA hybrid applications. (a) 2.5-D integration and (b) 3-D integration of logic and FPGA dice with integrated cooling on the interposer.

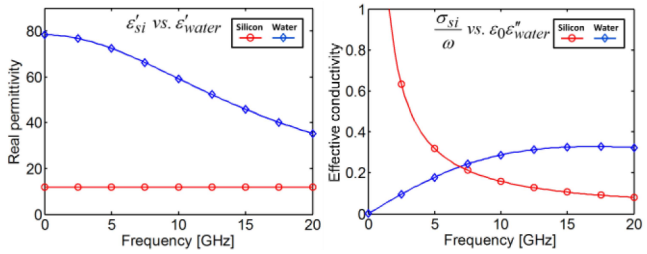

Fig. 2. Real permittivity and conductive property of silicon and distilled water as a function of frequency [9], [10].

cooling on the interposer. In such liquid-cooled systems, a signal propagating through the TSV will encounter capacitance partially through silicon and partially through distilled water. Unlike the permittivities of silicon, the permittivities of distilled water significantly vary over frequency [10]. Furthermore, distilled water becomes more conductive than silicon at high frequencies, as shown in Fig. 2, while it has approximately zero conductivity at dc. From Ampere's law (1), the complex permittivity, $\hat{\varepsilon}$, is defined as shown in (2)

$$\nabla \times \bar{H} = j\omega \cdot \hat{\varepsilon} \cdot \bar{E} \tag{1}$$

$$\hat{\varepsilon} = \varepsilon_0 \ \ \varepsilon_r \left(1 - j\frac{\sigma_{\text{eff}}}{\omega\varepsilon_0\varepsilon_r}\right) = \varepsilon_0\varepsilon_r(1 - j \cdot \tan\delta) \tag{2}$$

where ε_0, ε_r, ω, σ_{eff}, and $\tan\delta$ are the absolute dielectric permittivity, relative permittivity, angular frequency, effective conductivity, and loss tangent, respectively [19], [20]. The loss tangent can be divided into two parts

$$\tan\delta = \tan\delta_d + \tan\delta_c = \frac{\varepsilon''}{\varepsilon_r} + \frac{\sigma}{\omega\varepsilon_0\varepsilon_r} \tag{3}$$

where σ and ε'' are the conductivity and the imaginary permittivity of a substrate, respectively. Here, $\tan\delta_d$ represents the polarization loss of the substrate, and $\tan\delta_c$ represents the losses as a result of its conductivity [19]. For a silicon substrate, $\tan\delta_c$ dominates, since the conductivity of silicon is considerably higher (silicon is a semiconductor material), and thus, the first portion of (3) is ignored. On the other hand, for distilled water, $\tan\delta_d$ dominates, because the imaginary

TABLE I

SPECIFICATION OF SILICON AND DISTILLED WATER USED IN THE EXPERIMENTS

	Conductivity	Permittivity	Dissolved solids
Silicon	10 S/m	11.9	N/A
Distilled water	< 0.5 μS/cm	Follows Debye function [10]	< 0.5 ppm (total)

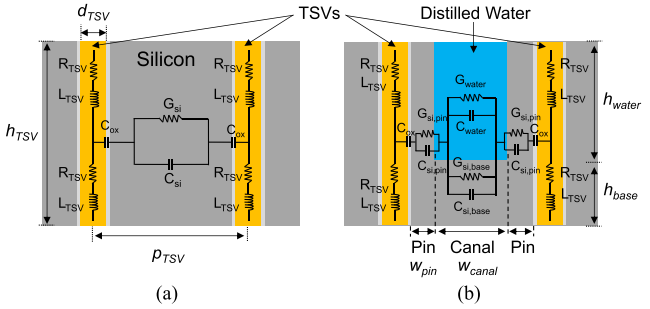

Fig. 3. Equivalent circuit models for (a) conventional TSVs in a silicon substrate and (b) TSVs in a micropin-fin heat sink within distilled water.

permittivity of distilled water, or ε'', is relatively high, while the conductivity of distilled water is negligible (<0.5 μS/cm, as shown in Table I). Thus, the complex permittivity of silicon and distilled water can be simplified as

$$\hat{\varepsilon}_{\text{si}} \approx \varepsilon_0\varepsilon_{\text{si}}\left(1 - j\frac{\sigma_{\text{si}}}{\omega\varepsilon_0\varepsilon_{\text{si}}}\right) = \varepsilon_0\varepsilon_{\text{si}} - j\frac{\sigma_{\text{si}}}{\omega} \tag{4}$$

$$\hat{\varepsilon}_{\text{water}} \approx \varepsilon_0\varepsilon_{\text{water}}\left(1 - j\frac{\varepsilon''_{\text{water}}}{\varepsilon_{\text{water}}}\right) = \varepsilon_0\varepsilon_{\text{water}} - j\varepsilon_0\varepsilon''_{\text{water}} \tag{5}$$

respectively. The second term of each equation refers to the effective conductivity of the material. Fig. 2 shows the real permittivity and the effective conductivity of silicon and distilled water, respectively [10]. It can be seen that the effective conductivity of distilled water exceeds the conductivity of silicon at frequencies greater than 6.7 GHz, while the real permittivity of distilled water is unceasingly higher than that of silicon. Fig. 3 shows the equivalent circuit models of conventional TSVs in a silicon substrate from [20] and TSVs in a micropin-fin heat sink within distilled water. It should be noted that, for the TSVs within distilled water, TSV capacitance and conductance are formed through not only silicon but also distilled water, as shown in Fig. 3(b). While the resistance and inductance of TSVs (R_{TSV} and L_{TSV}) remain consistent between the two models, the capacitance and the conductance of TSVs differ as follows. The capacitance and the conductance of Fig. 3(b) consist of both silicon and distilled water between signal and ground TSVs (i.e., the canal region). If the width of the canal region (w_{canal}) increases, or equivalently the width of the micropin-fin (w_{pin}) decreases, at a fixed TSV pitch, the amount of water between TSVs increases. From an electrical perspective, this would increase the overall TSV capacitance and conductance, because distilled water has higher permittivity and conductivity than silicon at high frequencies. Thus, when a liquid-cooled microsystem is designed, the microfluidic heat sink dimensions should be codesigned

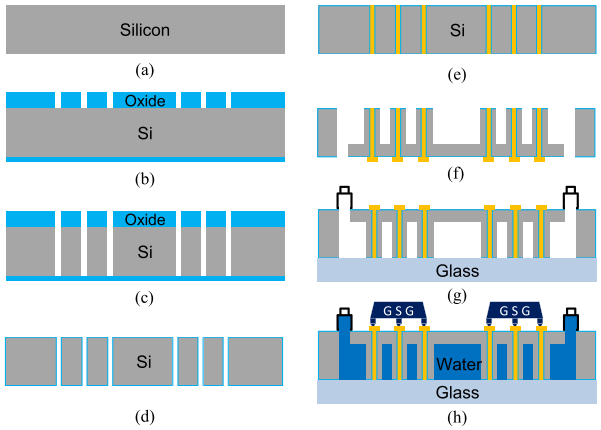

Fig. 4. Schematic of the overall fabrication process of TSVs embedded in a micropin-fin heat sink. (a) Double side polished silicon wafer. (b) Silicon dioxide deposition and anisotropy etching. (c) Etching via holes using the Bosch process. (d) Remaining oxide removal and wet oxidation. (e) Copper electroplating. (f) Fabrication of a micropin-fin structure using the Bosch process. (g) Assembly of the fabricated testbed, a glass slide, and fluidic I/Os. (h) High-frequency measurements with distilled water.

with respect to the TSVs, which will be analyzed in the sections IV and V.

III. Microfabrication of a Micropin-Fin Heat Sink With Embedded TSVs

This section presents the microfabrication of TSVs embedded in three sets of micropin-fins for the high-frequency characterization of TSVs. Fig. 4 shows the overall fabrication process of the TSVs in a micropin-fin heat sink. The process begins with the deposition of silicon dioxide (∼9 μm), followed by the deposition of metal using an e-beam evaporator. In this process, a thin layer of chrome (∼0.5 μm) is chosen as an etch mask [Fig. 4(b)], since it has significantly high selectivity over silicon dioxide [21]. After etching the silicon dioxide layer through the chrome mask, the remaining chrome is removed using a CR-7S chrome etchant. Using the resulting silicon dioxide as an etch mask, the high-aspect ratio Bosch process [22] is performed to etch via holes through the silicon wafer [Fig. 4(c)].

Following the removal of any remaining silicon dioxide etch mask, wet oxidation is performed to isolate the vias from the silicon substrate [Fig. 4(d)]. Next, titanium and copper (30/500 nm) seed layers are deposited using an e-beam evaporator at the back side of the wafer. To pinchoff the etched openings, copper electroplating is performed at the back side using dc bias. Next, bottom–up copper electroplating is performed from the front side of the wafer with a pulsed mode power supply (60:40 duty cycle). To remove the overburden copper after electroplating, chemical mechanical polishing (CMP) is performed from both sides of the wafer [Fig. 4(e)]. Following CMP, metal pads consisting of titanium, copper, and gold (30/2000/100 nm) are selectively deposited using an e-beam evaporator to facilitate probing. The Bosch process is performed to fabricate a silicon micropin-fin heat sink structure around the TSVs [Fig. 4(f)]. Fig. 5 shows SEM images of three diameters (50, 100, and 150 μm) of micropin-fins each with a single TSV. The height and the base thickness of the micropin-fins are 230 and 100 μm, respectively. TSV diameter, pitch, and height are 13, 200, and 330 μm, respectively. Lastly, the fabricated testbed is assembled to a glass slide with fluidic inlet/outlets for fluid delivery [Fig. 4(g)].

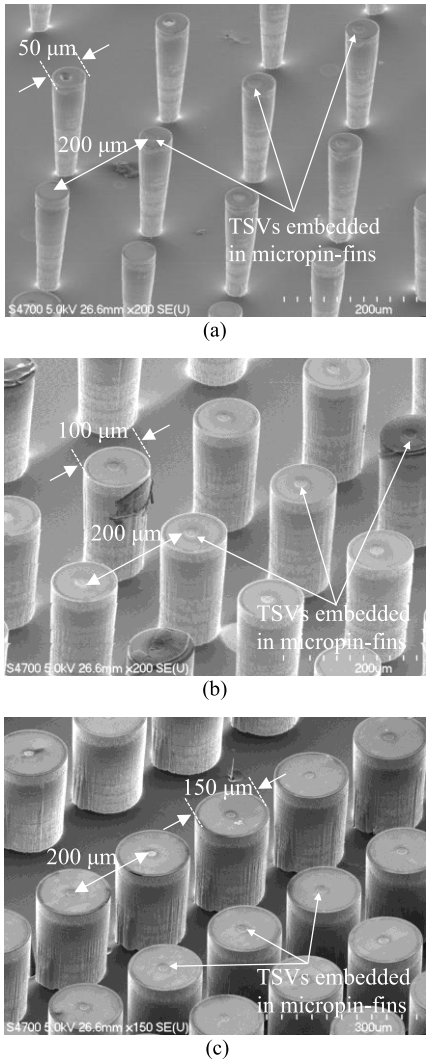

Fig. 5. SEM images of the fabricated micropin-fins with embedded TSVs. Micropin-fin diameters of (a) 50, (b) 100, and (c) 150 μm. The TSV pitch is fixed at 200 μm (each micropin-fin contains one TSV).

IV. High-Frequency Characterization of TSVs in a Micropin-Fin Heat Sink Within Distilled Water

To characterize the high-frequency behavior of TSVs in distilled water, the fabricated testbed described in Section III was filled with distilled water, as shown in Fig. 4(h). Fig. 6 shows the used high-frequency characterization setup, including the testbed, a microprobe station with Cascade $|Z|$ probes, and an Agilent N5245A PNA-X network analyzer. To extract TSV capacitance and conductance from the measurements, single-port characterization of ground-signal-ground (GSG) TSVs is performed. TSVs are open-terminated at the bottom side (where it meets the glass slide). Fig. 7 shows the magnitude and the phase of S_{11} from the measurements and 3-D full-wave simulation of TSVs in a silicon substrate and TSVs within distilled water, respectively. After the S-parameter (S_{11}) to Z-parameter (Z_{11}) conversion using (6), TSV capacitance

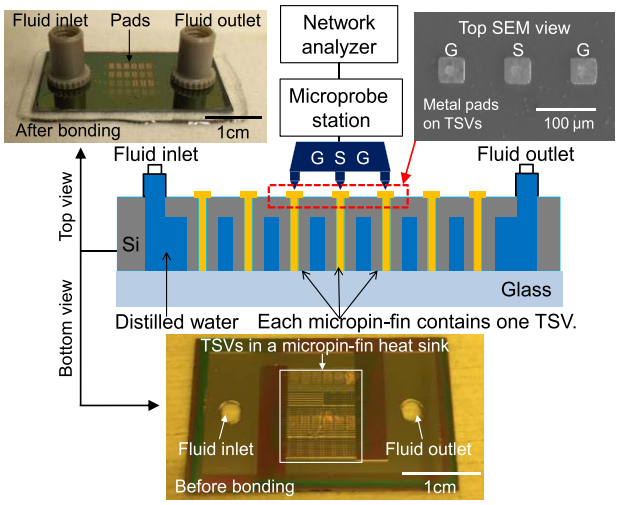

Fig. 6. Schematic of the high-frequency characterization setup for TSVs within distilled water.

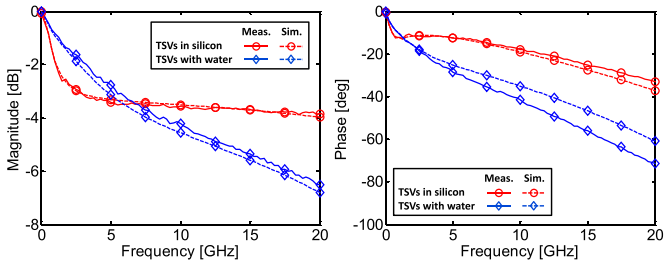

Fig. 7. Magnitude and phase of S_{11} of TSVs in a silicon substrate and TSVs within a micropin-fin heat sink filled within distilled water (measurement and simulation).

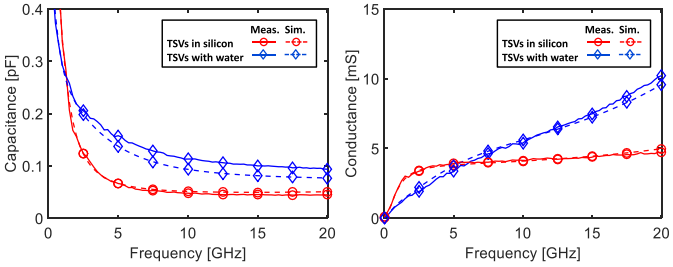

Fig. 8. Extracted capacitance and conductance of TSVs in a silicon substrate and TSVs within a micropin-fin heat sink filled within distilled water (measurement and simulation).

and conductance are extracted from Z_{11} using (7) and (8)

$$Z_{11} = Z_0 \cdot \frac{1 + S_{11}}{1 - S_{11}} \tag{6}$$

$$C_{\mathrm{TSV}} = \frac{1}{\mathrm{Im}(Z_{11}) \cdot \omega} \tag{7}$$

$$G_{\mathrm{TSV}} = \frac{1}{\mathrm{Re}(Z_{11})} \tag{8}$$

where Z_0 is the characteristic impedance [23], [24]. The extracted capacitance and the conductance of TSVs in a silicon substrate and TSVs within a micropin-fin heat sink with distilled water are compared through measurement and simulation, as shown in Fig. 8 and Table II. As shown in Fig. 2, the permittivity of distilled water is always higher than silicon

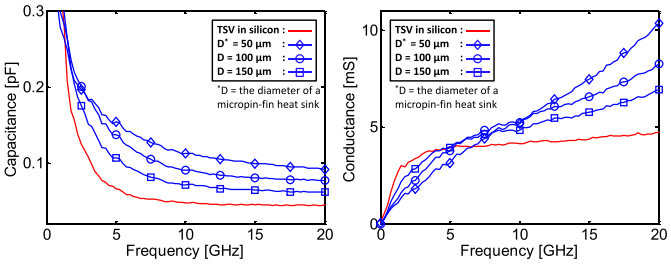

Fig. 9. Extracted capacitance and conductance of TSVs within distilled water as a function of the micropin-fin diameter from measurements. TSVs in micropin-fins with three diameters (50, 100, and 150 μm) at a fixed TSV pitch of 200 μm are compared.

TABLE II

EXTRACTED CAPACITANCE AND CONDUCTANCE FROM SIMULATION AND MEASUREMENT OF TSVS IN A SILICON SUBSTRATE (SILICON) AND IN A MICROPIN-FIN HEAT SINK WITHIN DISTILLED WATER (WATER)

Substrate (@ 20 GHz)	Capacitance [fF]		Conductance [mS]	
	Silicon	Water	Silicon	Water
Simulation	49.9	77.1	4.9	9.2
Measurements	44.7	91.5	4.7	10.4

TABLE III

EXTRACTED CAPACITANCE AND CONDUCTANCE FOR EACH CASE. TSVS IN A SILICON SUBSTRATE AND TSVS WITHIN DISTILLED WATER FOR DIFFERENT MICROPIN-FIN DIAMETERS AT THE FIXED TSV PITCH

Substrate (@ 20GHz)	Silicon	D* = 150 μm	D = 100μm	D = 50μm
Extracted capacitance [fF]	44.8	62.0	76.9	91.5
Extracted conductance [mS]	4.7	6.9	8.3	10.4

*D = the diameter of a silicon micropin-fin heat sink.

permittivity; however, the effective conductivity of distilled water is initially lower than silicon conductivity and becomes higher as frequency increases. In Fig. 8, it can be seen that the capacitance of TSVs within distilled water is lower at low frequencies than the capacitance of TSVs in silicon. This is because the extracted equivalent capacitance is a function of both capacitance and conductance of the materials [23]. As frequency increases, the capacitance of TSVs within distilled water remains higher than TSVs in a silicon substrate. Similarly, the conductance of TSVs within distilled water is lower than TSVs in silicon at frequencies lower than approximately 5 GHz, but becomes more conductive at higher frequencies. To quantitatively analyze this behavior, the three measurements of TSVs in micropin-fins with different diameters (50, 100, and 150 μm) are compared at a fixed TSV pitch of 200 μm, as shown in Fig. 9 and Table III. Each plot compares the extracted capacitance and conductance, respectively, from measurements for all cases (TSVs in silicon and TSVs in the three different diameters of micropin-fins). The results show that as the diameter of micropin-fins decreases, or equivalently as the volume of water between TSVs increases, TSV capacitance increases because of the

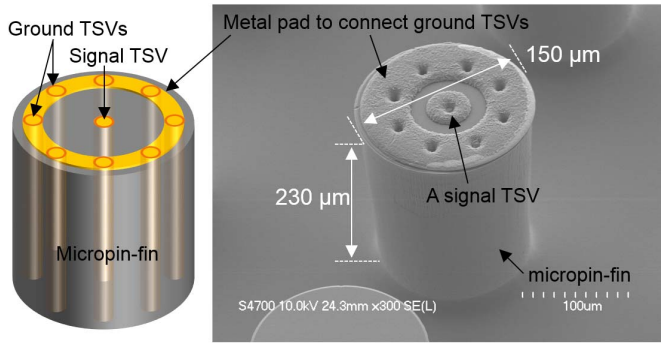

Fig. 10. Schematic and SEM image of coaxial-like TSVs in a micropin-fin heat sink. Multiple ground TSVs surround a center signal TSV.

high permittivity of distilled water. However, the conductance of TSVs within distilled water initially decreases as the volume of water increases at low frequency. On the contrary, at higher frequencies, the data show that the conductance increases as the amount of water increases, as shown in Fig. 9. This can be attributed to the conductive property of distilled water, which is less conductive than silicon at low frequency but more conductive than silicon at high-frequency [8]. Moreover, this property of distilled water will significantly change the characteristic impedance of TSVs, which is a function of capacitance and conductance. The results imply that a micropin-fin heat sink geometry, or a microfluidic heat sink design, is one of the critical factors that determines the electrical performance of TSVs. Thus, for liquid-cooled microsystems that require invariant signal transmission, signal TSVs should be isolated from such variations, which is addressed in Section V.

V. Coaxial-like TSV Configuration to Shield the Effect of Distilled Water

In this section, we propose a TSV configuration whose electrical attributes are invariant to the coolant or surroundings. A coaxial TSV configuration is a well-known solution to suppress undesirable substrate loss, noise, and coupling as well as provide excellent impedance matching [20], [25], [26]. However, the main limitation of coaxial TSVs is the high complexity of fabrication, which requires extra polymer material, BCB or SU-8, between signal and ground layers [20], [26]. Moreover, the dimension of the cylindrical ground layer is typically large compared to TSVs, which results in different silicon etching and copper filling rates.

To address such issues, we propose a coaxial-like TSV configuration that consists of multiple ground TSVs (instead of a cylindrical layer) surrounding a signal TSV of the same copper dimension, as shown in Fig. 10. In this configuration, a silicon micropin-fin consists of a single center signal TSV surrounded by multiple ground TSVs, and an annular-shaped metal pad connects all ground TSVs. The single-port measurements of coaxial-like TSVs are performed under two conditions: 1) coaxial-like TSVs in silicon and 2) coaxial-like TSVs in a micropin-fin within distilled water. To validate the shielding effect of coaxial-like TSVs, the S_{11} values of both cases are measured and shown in Fig. 11(a). The expectation is

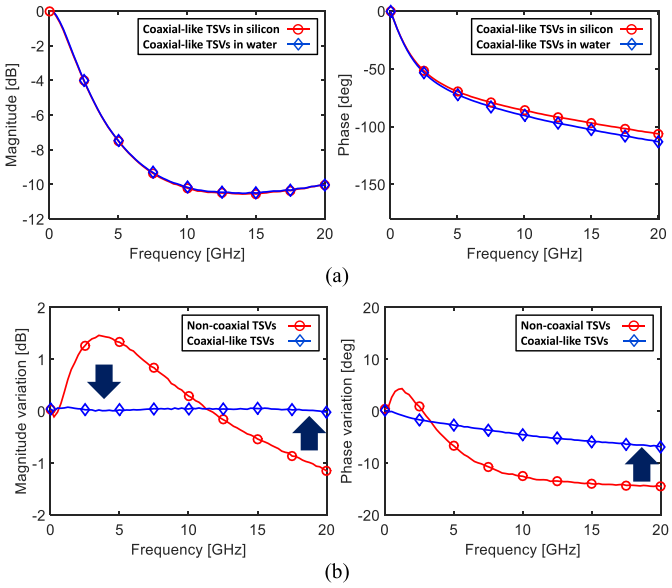

Fig. 11. (a) S_{11} magnitude and phase of coaxial-like TSVs. (b) Variations of S_{11} magnitude and phase. Coaxial-like TSVs exhibit shielding effects, showing less variation than noncoaxial TSVs.

approximately no variations between two measurements in S-parameters if coaxial-like TSVs have good shielding. In addition, noncoaxial TSVs, which consist of a single TSV in each micropin-fin (without ground TSVs), are also measured and compared under the same conditions. The measured S-parameters of each case are subtracted, and magnitude and phase variations are shown in Fig. 11(b). In the plot, the magnitude difference of coaxial-like TSVs was less than ± 0.1 dB due to the ground shielding effect, while ± 1.3-dB magnitude difference was observed when there is no shielding TSVs. The results show that the ground TSVs (in the coaxial-like TSV case) successfully shield the signal transmission through the center signal TSV. Moreover, phase difference of 65.8% was alleviated due to the ground shielding effect. The coaxial-like TSVs exhibit a phase difference of $\sim 6^\circ$ at 20 GHz, and this is believed to be caused by the nonperfect coaxial structure of the TSVs. Thus, when a stable signal transmission is required in a liquid-cooled 3-D microsystem, the coaxial-like TSVs should be utilized to shield the signal TSVs.

VI. Conclusion

This paper, for the first time, experimentally analyzes the electrical performance of TSVs within distilled water for liquid-cooled microsystems. This paper presents the fabrication of three diameters (50, 100, and 150 μm) of a silicon micropin-fin heat sink with embedded TSVs. The fabricated testbed was assembled with a glass slide and filled with distilled water. The single-port measurements of GSG TSVs were performed for two cases: 1) conventional TSVs in a silicon substrate and 2) TSVs within a micropin-fin heat sink surrounded by distilled water. The results demonstrate that TSVs within distilled water have larger capacitance and conductance than TSVs in a silicon substrate due to the lossy characteristics of distilled water. As the volume of distilled water increases between TSVs at a fixed TSV pitch,

TSV capacitance and conductance increase at high frequency. Moreover, we propose and demonstrate a coaxial-like TSV configuration, which consists of multiple ground TSVs surrounding a center signal TSV, to shield signal TSVs from electrical variations caused by the working fluid.

REFERENCES

[1] R. S. Patti, "Three-dimensional integrated circuits and the future of system-on-chip designs," *Proc. IEEE*, vol. 94, no. 6, pp. 1214–1224, Jun. 2006.

[2] T. Brunschwiler *et al.*, "Interlayer cooling potential in vertically integrated packages," *Microsyst. Technol.*, vol. 15, pp. 57–74, Aug. 2008.

[3] S. V. Garimella, V. Singhal, and D. Liu, "On-chip thermal management with microchannel heat sinks and integrated micropumps," *Proc. IEEE*, vol. 94, no. 8, pp. 1534–1548, Aug. 2006.

[4] D. B. Tuckerman and R. F. W. Pease, "High-performance heat sinking for VLSI," *IEEE Electron Device Lett.*, vol. 2, no. 5, pp. 126–129, May 1981.

[5] S. Ndao, Y. Peles, and M. K. Jensen, "Multi-objective thermal design optimization and comparative analysis of electronics cooling technologies," *Int. J. Heat Mass Transf.*, vol. 52, nos. 19–20, pp. 4317–4326, 2009.

[6] M. S. Bakir *et al.*, "3D heterogeneous integrated systems: Liquid cooling, power delivery, and implementation," in *Proc. Custom Integr. Circuits Conf.*, 2008, pp. 663–670.

[7] Y. Zhang, A. Dembla, and M. S. Bakir, "Silicon micropin-fin heat sink with integrated TSVs for 3-D ICs: Tradeoff analysis and experimental testing," *IEEE Trans. Compon., Packag., Manuf. Technol.*, vol. 3, no. 11, pp. 1842–1850, Nov. 2013.

[8] D. Eisenberg and W. Kauzmann, *The Structure and Properties of Water*. New York, NY, USA: Oxford Univ. Press, 1969.

[9] W. J. Ellison, "Permittivity of pure water, at standard atmospheric pressure, over the frequency range 0–25 THz and the temperature range 0–100 °C," *J. Phys. Chem. Ref. Data*, vol. 36, no. 1, pp. 1–18, 2007.

[10] U. Kaatze, "Complex permittivity of water as a function of frequency and temperature," *J. Chem. Eng. Data*, vol. 34, no. 4, pp. 371–374, Oct. 1989.

[11] C. Song and P. Wang, "A radio frequency device for measurement of minute dielectric property changes in microfluidic channels," *Appl. Phys. Lett.*, vol. 94, no. 2, p. 023901, 2009.

[12] M. S. Kheir, H. F. Hammad, and A. S. Omar, "Measurement of the dielectric constant of liquids using a hybrid cavity-ring resonator," in *Proc. PIERS*, 2008, pp. 566–569.

[13] O. L. Chlieh, W. T. Khan, and J. Papapolymerou, "L-band tunable microstrip bandpass filter on multilayer organic substrate with integrated microfluidic channel," in *Proc. IEEE MTT-S Int. Microw. Symp. (IMS)*, Jun. 2014, pp. 1–4.

[14] Y. Cui, J. Sun, Y. He, Z. Wang, and P. Wang, "A simple, tunable, and highly sensitive radio-frequency sensor," *Appl. Phys. Lett.*, vol. 103, no. 6, p. 062906, 2013.

[15] A. Kozhevnikov, "Wideband radio-frequency device for measurements of dielectric properties of small volumes of liquids," *Meas. Sci. Technol.*, vol. 21, no. 4, p. 043001, 2010.

[16] C.-H. Chen, D. J. Chung, S. Bhattacharya, J. Papapolymerou, and D. Peroulis, "Low-cost 3-D integration of RF and micro-cooling systems," in *Proc. 38th Eur. Microw. Conf.*, Oct. 2008, pp. 9–12.

[17] T. E. Sarvey, Y. Zhang, Y. Zhang, H. Oh, and M. S. Bakir, "Thermal and electrical effects of staggered micropin-fin dimensions for cooling of 3D microsystems," in *Proc. 14th IEEE Intersoc. Conf. Thermal Thermomech. Phenomena Electron. Syst. (ITherm)*, May 2014, pp. 205–212.

[18] B. Curran, I. Ndip, S. Guttovski, and H. Reichl, "The impacts of dimensions and return current path geometry on coupling in single ended through silicon vias," in *Proc. 59th Electron. Compon. Technol. Conf.*, May 2009, pp. 1092–1097.

[19] D. M. Pozar, *Microwave Engineering*, 3rd ed. New York, NY, USA: Wiley, 2005.

[20] I. Ndip *et al.*, "High-frequency modeling of TSVs for 3-D chip integration and silicon interposers considering skin-effect, dielectric quasi-TEM and slow-wave modes," *IEEE Trans. Compon., Packag., Manuf. Technol.*, vol. 1, no. 10, pp. 1627–1641, Oct. 2011.

[21] K. R. Williams, K. Gupta, and M. Wasilik, "Etch rates for micromachining processing—Part II," *J. Microelectromech. Syst.*, vol. 12, no. 6, pp. 761–778, Dec. 2003.

[22] H. Oh, J. M. Gu, S. J. Hong, G. S. May, and M. S. Bakir, "High-aspect ratio through-silicon vias for the integration of microfluidic cooling with 3D microsystems," *Microelectron. Eng.*, vol. 142, pp. 30–35, Jul. 2015.

[23] Y. Eo and W. R. Eisenstadt, "High-speed VLSI interconnect modeling based on s-parameter measurements," *IEEE Trans. Compon., Hybrids, Manuf. Technol.*, vol. 16, no. 5, pp. 555–562, Aug. 1993.

[24] I. Ndip *et al.*, "Analytical, numerical-, and measurement-based methods for extracting the electrical parameters of through silicon vias (TSVs)," *IEEE Trans. Compon., Packag., Manuf. Technol.*, vol. 4, no. 3, pp. 504–515, Mar. 2014.

[25] F. Liang, G. Wang, D. Zhao, and B.-Z. Wang, "Wideband impedance model for coaxial through-silicon vias in 3-D integration," *IEEE Trans. Electron Devices*, vol. 60, no. 8, pp. 2498–2504, Aug. 2013.

[26] Z. Xu and J.-Q. Lu, "Three-dimensional coaxial through-silicon-via (TSV) design," *IEEE Electron Device Lett.*, vol. 33, no. 10, pp. 1441–1443, Oct. 2012.

Hanju Oh (S'14) received the B.S. degree in electrical and computer engineering from Hanyang University, Seoul, Korea, in 2010, and the M.S. degree from the Georgia Institute of Technology, Atlanta, GA, USA, in 2014, where he is currently pursuing the Ph.D. degree in electrical and computer engineering.

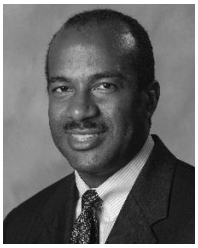

Gary S. May (F'06) received the B.S. degree in electrical engineering from the Georgia Institute of Technology (Georgia Tech), Atlanta, GA, USA, in 1985, and the M.S. and Ph.D. degrees in electrical engineering and computer science from the University of California at Berkeley, Berkeley, CA, USA, in 1987 and 1991, respectively.

He is currently the Dean of the College of Engineering at Georgia Tech.

Muhannad S. Bakir (SM'12) received the B.E.E. degree from Auburn University, Auburn, AL, USA, in 1999, and the M.S. and Ph.D. degrees in electrical and computer engineering from the Georgia Institute of Technology (Georgia Tech), Atlanta, GA, USA, in 2000 and 2003, respectively.

He is currently an Associate Professor with the School of Electrical and Computer Engineering, Georgia Tech.